Supramolecular Assemblies of Polybenzimidazole and Aromatic Polycarboxylic Acids with Superior Mechanical and H2/CO2 Separation Properties

SCHOLARONE™
Manuscripts

Supramolecular Assemblies of Polybenzimidazole and Aromatic Polycarboxylic Acids with Superior Mechanical and H$_2$/CO$_2$ Separation Properties

Leiqing Hu,[a] Vinh T. Bui,[a] Shouhong Fan,[b] Wenji Guo,[a] Sankhajit Pal,[a] Yifu Ding,[b] and Haiqing Lin*[a]

Aromatic polycarboxylic acids complex with imidazoles, forming supramolecular assemblies. Herein, we demonstrate that polybenzimidazole (PBI) can be augmented by aromatic polycarboxylic acids, including phthalic acid (PA), trimesic acid (TMA), and pyromellitic acid (PMA), and the resulting supramolecular assemblies exhibit attractive H$_2$/CO$_2$ separation performance for precombustion carbon capture. The acid doping decreases the free volume and gas permeability but increases H$_2$/CO$_2$ selectivity, which can be correlated with the molar ratio of the protons to PBI repeating units in the assemblies. Increasing the temperature decreases the H$_2$/CO$_2$ selectivity because of the weakened interactions. When challenged with model gas mixtures, a supramolecular assembly based on TMA shows H$_2$/CO$_2$ separation properties superior to state-of-the-art materials and above Robeson's upper bound. This study elucidates the fruitful harness of dynamic non-covalent bonds to design robust and highly selective membranes for industrial gas separations.

Introduction

Blue hydrogen has been proposed as one of the key energy carriers to transform our fossil fuel-based society into a carbon-negative one, and it can be produced at a large scale by reforming or gasification of fossil fuels while the byproduct CO$_2$ is captured for utilization or sequestration. Membrane technology has emerged as a leading technology for H$_2$/CO$_2$ separation owing to its inherent advantages of great energy efficiency, small footprint, and easy scalability, operation, and maintenance.[1-4] Membranes should exhibit high H$_2$ permeability and high H$_2$/CO$_2$ selectivity at elevated temperatures (150 °C and above) for them to be competitive with conventional technologies such as absorption or adsorption. Specifically, membrane materials should have a strong size-sieving ability to achieve high selectivity because H$_2$ (with a kinetic diameter of 2.89 Å) is smaller than CO$_2$ (3.3 Å).[5-8]

Glassy polymers with low free volume have been extensively explored for H$_2$/CO$_2$ separation. For example, polybenzimidazole (PBI) exhibits H$_2$/CO$_2$ selectivity of 12-16 at 150 °C because of the suitable free volume sizes derived from hydrogen bonds and π-π stacking.[9, 10] Polymers can be further chemically cross-linked to tighten chain packing and thus increase the size-sieving ability and thus H$_2$/CO$_2$ selectivity.[2, 11] For example, PBI was cross-linked through the reaction of the amine groups and terephthaloyl chloride or 1,3,5-tris(bromomethyl)benzene to increase H$_2$/CO$_2$ selectivity to ≈ 24 at 150 °C;[12, 13] polyimides of P84[14] and 6FDA-durene[15-18] were cross-linked using diamines; and polymers of intrinsic microporosity (PIMs) were cross-linked by UV[19] or heat.[20] However, the chemical cross-linking leads to heterogeneous structures and decreases

extensibility.[21] The conventional post-cross-linking also results in a gradient of cross-linking density from the surface to the center of the films.

Recently, dynamic cross-linking of polymers using non-covalent bonds such as reversible hydrogen bonds (H-bonds) to form supramolecular assemblies has attracted significant interest because it can improve stiffness and molecular separation properties without significantly reducing the extensibility and toughness.[21-23] For example, PBI was doped with inorganic polyprotic acids, including phosphoric acids (H$_3$PO$_4$), sulfuric acid (H$_2$SO$_4$), and pyrophosphoric acid (H$_4$P$_2$O$_7$, PpA),[5, 24] and aliphatic polycarboxylic acids, including oxalic acid (C$_2$H$_2$O$_4$, OA) and trans-aconitic acid (C$_6$H$_6$O$_6$, TaA).[25] These acids form multiple H-bonds with the imidazoles on the PBI backbones, effectively decreasing the free volume and H$_2$ permeability but significantly increasing the H$_2$/CO$_2$ selectivity.

Interestingly, imidazoles can complex with aromatic polycarboxylic acids (such as isophthalic acid), forming salts[26, 27] (due to H-bonds and proton transfer) or co-salts (because of the H-bonds).[28] For instance, benzimidazole and isophthalic acid (with a molar ratio of 1:1) formed co-crystal or supramolecular structures.[28] However, to the best of our knowledge, such interactions have never been exploited to tailor the physical properties of PBI for gas separations.

In this study, we systemically investigated PBI-based supramolecular assemblies for H$_2$/CO$_2$ separation, which are derived from three aromatic polycarboxylic acids, including phthalic acid (PA), trimesic acid (TMA), and pyromellitic acid (PMA), as shown in Fig. 1. In addition to the H-bonds and proton transfer, the addition of these aromatic acids can also introduce the π-π interactions, improving the PBI chain packing. The supramolecular assemblies are named PBI-acid$_x$, where x represents the doping level defined as the molar ratio of the acid to PBI repeating units in the films. These acids have similar structures and acidity but different proton numbers (cf. Table S1), rendering good models to study the effect of H-bonding

[a]Department of Chemical and Biological Engineering, University at Buffalo, The State University of New York, Buffalo, NY 14260, USA. Email: haiqingl@buffalo.edu
[b]Department of Mechanical Engineering, University of Colorado, Boulder, CO 80309, USA
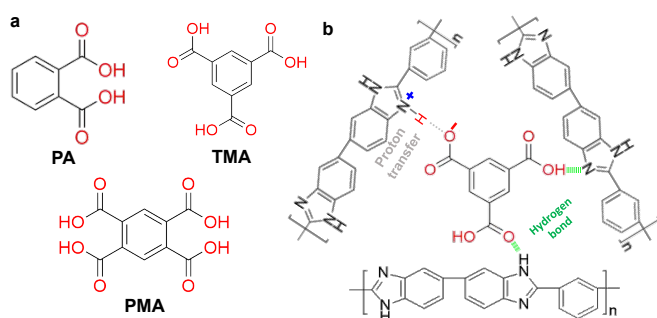
Fig. 1 (a) Chemical structures of PA, TMA, and PMA. (b) Schematic illustration of the PBI-TMA supramolecular assembly.

interactions on thermal, mechanical, and H_2/CO_2 separation properties. The effects of the doping level and temperature on the H_2/CO_2 separation properties are thoroughly determined. The samples with the best H_2/CO_2 separation properties are further challenged with model syngas and demonstrate superior H_2/CO_2 separation performance above Robeson's upper bound and their potential for practical applications.

Experimental

Materials

Celazole® PBI (S10) was acquired from PBI Performance Products Inc. (Charlotte, NC). PA, TMA, and PMA were procured from Sigma-Aldrich Corporation (St. Louis, MO). Methanol (99.8%) was obtained from Fisher Scientific (Waltham, MA).

Preparation of acid-doped PBI films

PBI films of ≈12 μm were prepared from the S10 solution using a solution casting method.[25] The films were dried at 200 °C under vacuum for 48 h followed by immersion in methanol at ≈ 23 °C for 24 h to remove any residual DMAc. The film was finally dried at 100 °C to remove methanol. To conduct acid-doping, PBI films were immersed in methanol solutions containing the desired amount of acid at ≈ 23 °C. The exposure time was set at 48 h for PA and 168 h for TMA and PMA to ensure the equilibrium of the acid and PBI reaction (c.f. Fig. 1b). After that, the film was dried at 100 °C under vacuum for 12 h. The doping level (x) is calculated using the following equation:

$$x = \left(\Delta m/M_a\right)\big/\left(m_0/M_p\right) \qquad (1)$$

where m_0 and Δm are the mass of the dry sample before the acid doping and the mass increase after acid doping, respectively. M_a and M_p are the molar mass of the acid (PA: 166 g mol^{-1}; TMA: 210 g mol^{-1}; PMA: 254 g mol^{-1}) and the PBI repeating unit (308 g mol^{-1}), respectively.

Characterization of acid-doped PBI films

Fourier transform infrared (FTIR) spectra of the samples from 1000 to 2000 cm^{-1} were acquired using a vertex 70 Burker spectrometer (Bruker Scientific LLC, Billerica, MA). Wide-angle X-ray diffraction (WAXD) patterns were obtained from 5 – 45° using a Rigaku Ultima

IV X-ray diffractometer (Rigaku Analytical Devices, Wilmington, MA) with CuKα. An SDT Q600 thermogravimetric analyzer (TA Instruments, New Castle, DE) was used to determine thermal properties up to 800 °C at a ramping rate of 10 °C/min under N_2 flow.

The mechanical properties of the samples were determined using static tensile loading at 35 and 100 °C by a dynamic mechanical analysis (DMA, Q800 TA Instrument). The sample (20 mm × 2.5 mm) was applied uniaxial tensile loading with an initial strain of 0.1% at 1.0%/min till the sample fractured. Young's modulus was determined from the elastic deformation region of the stress-strain curve. The tensile strength and fracture strain can also be determined using the stress-strain curve.

The density of the pure acids was determined using a Micromeritics Accu-Pyc II 1340 Gas Pycnometer (Micromeritics Instrument Corporation, Norcross, GA). The density of the PBI-acid films was calculated from their mass in the air and iso-octane based on the Archimedes' principle.[25, 29]

Pure-gas permeability was determined using a constant-volume and variable-pressure apparatus or a constant-pressure and variable-volume apparatus.[25] The permeability values from the two methods have the difference within 5%, less than their uncertainty (10%) estimated using the error propagation method.[25] Mixed-gas permeability was determined using a constant-pressure and variable-volume apparatus with gas chromatography to determine the compositions of the mixed-gas streams. Gas sorption isotherms of the PBI-acid samples were determined using a gravimetric sorption analyzer of IGA 001 (Hiden Isochema, Warrington, UK).[25, 29]

Results and discussion

Effect of the acid doping on physical properties

Fig. 2a exhibits the effect of the exposure time on the doping level of three acids in PBI. The doping reaches equilibrium after 72 h for PA and 168 h for TMA and PMA. PA requires the least time to reach the equilibrium probably because of its smallest molecular size, fewest carboxylic acid groups, and symmetric molecular structure. For example, PA has a molecular size (104 cm^3/mol, cf. Table S1), smaller than TMA (146 cm^3/mol) and PMA (160 cm^3/mol). The doping level (x) increases with the increasing amount of the acid in the doping solutions (cf. Fig. S1a), though the x values are lower than the molar ratio of the acid to PBI repeating units in the solutions because of the limitation by the reaction equilibrium. After acid doping, the films show appearance (cf. Fig. S2) and flexibility similar to the PBI films.

Fig. 2b displays the FTIR spectra of representative samples (PBI-PA$_{0.49}$, PBI-TMA$_{0.22}$, and PBI-PMA$_{0.16}$). These samples exhibit a new characteristic peak of $-COO^-$ at ≈1570 cm^{-1}, suggesting the proton transfer from $-COOH$ to the imidazole rings on the PBI backbones.[30] Moreover, the C$-$N stretching at 1620 cm^{-1} for PBI shifts to 1640 cm^{-1} for the PBI-acids because of the newly formed H-bonds.[25, 31] These results confirm the cross-linking mechanisms elucidated in Fig. 1b. The spectra also exhibit the characteristic peaks of $-COOH$ at ≈1680 cm^{-1}. This phenomenon can be ascribed to the high doping levels in PBI-PA$_{0.49}$; while for the PBI-TMA and PBI-PMA, it can be caused by
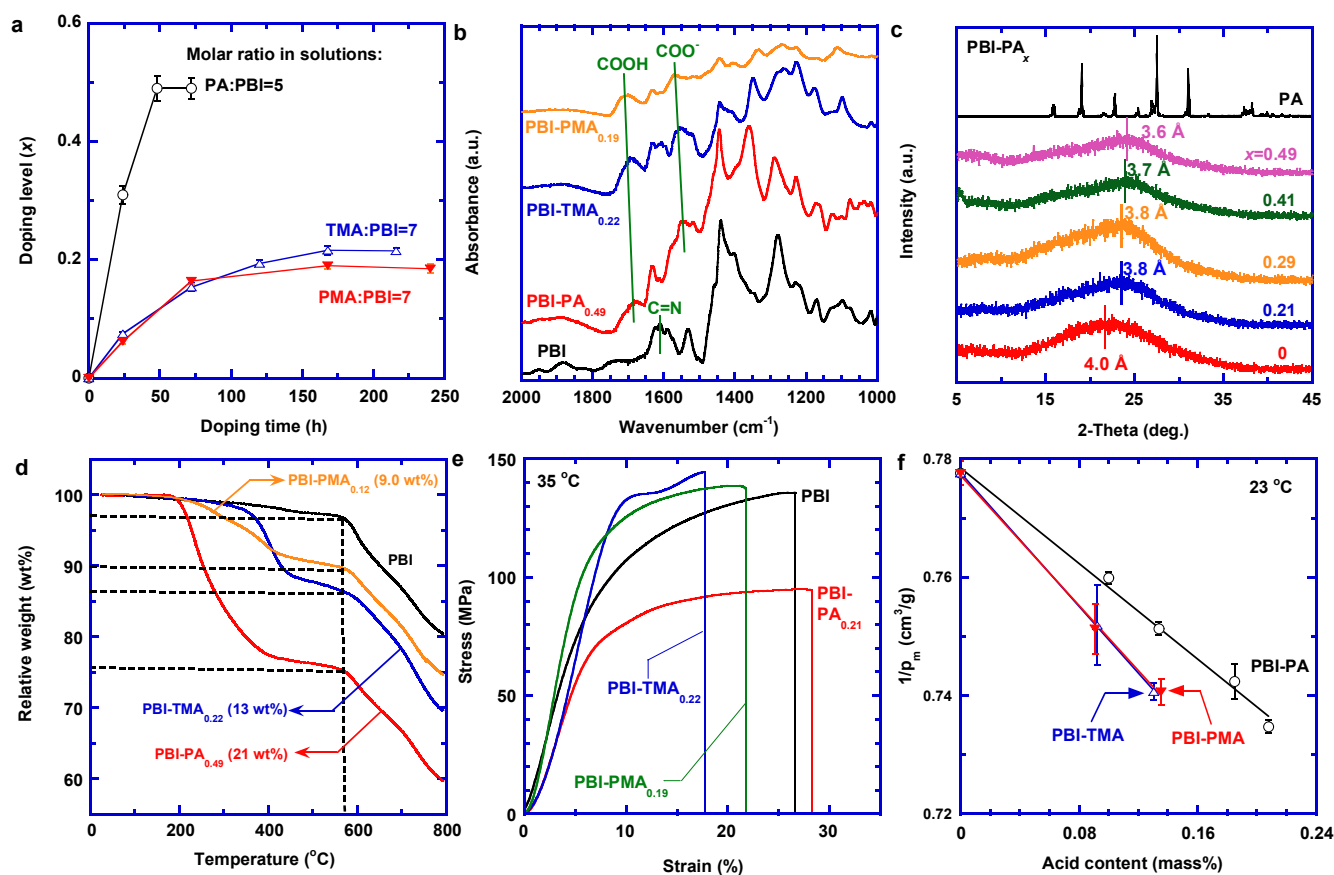
Fig. 2 Chemical and physical properties of PBI-acid samples. (a) Doping level of the acids in the PBI films as a function of the doping time. The molar ratio of the acid to the PBI repeating units in the solution is 5 for PA and 7 for TMA and PMA. (b) FTIR spectra. (c) WAXD patterns. (d) TGA curves. (e) Stress and strain plots at 35 °C. (f) Effect of the acid content on the density modelled using Eq. (2).

the third or fourth −COOH group with a high pK_a value and thus weak interactions with the imidazole rings.

Fig. 2c displays the WAXD patterns of the PBI-acids. Compared with the pure crystalline acids exhibiting sharp peaks (cf. Fig. S1b), the PBI-acids appear to be amorphous, suggesting that the acids become amorphous when interacting with PBI in the supramolecular assemblies. Additionally, PBI has a broad peak at 22°, corresponding to a d-spacing of 4.0 Å according to Bragg's equation.[29] The acid doping generally decreases the d-spacing, indicating the tightened polymer chain packing, though the change in the d-spacing is not substantial. For instance, PBI-PA$_{0.21}$ and PBI-PA$_{0.29}$ have very similar d-spacing values due to their similar doping levels. Nevertheless, PBI-PA$_{0.49}$ exhibits a d-spacing of 3.6 Å, lower than PBI, and the difference of 0.4 Å is similar to the kinetic diameter difference of the H_2 and CO_2. The same trend is also observed for PBI-TMA and PBI-PMA (Fig. S1c and Table S2).

Fig. 2d presents the TGA curves for representative samples, including PBI, PBI-PA$_{0.49}$, PBI-TMA$_{0.22}$, and PBI-PMA$_{0.12}$. PBI displays a mass loss of ~ 3% at 580 °C, similar to those reported in the literature, which can be attributed to the partial degradation of the impurities in the commercial PBI product.[13, 32] All samples are stable at temperatures up to 200 °C, indicating their potential for the H_2/CO_2 separation at 200 °C. The PBI-acid samples exhibit T$_{d,10\%}$ (defined as

the degradation temperature with 10% mass loss), much higher than the corresponding pure acids, which is consistent with the interactions between the acids and PBI as shown by the FTIR spectra. Additionally, in the absence of the interactions in the PBI-based blends, thermal properties of each component were shown to be independent from each other.[33, 34] Additionally, the acids in the complexes do not completely degrade until 580 °C, much higher than that for the pure acid (~200 °C for PA and PMA and ~300 °C for TMA). Interestingly, PBI-TMA samples exhibit higher T_d values than PBI-PA and PBI-PMA, consistent with the higher T_d for TMA than PA and PMA (Fig. S1d). PBI-PA$_{0.49}$, PBI-TMA$_{0.22}$, and PBI-PMA$_{0.12}$ show the mass loss of 10%, 14%, and 24% at 580 °C, respectively, consistent with the acid content in the samples assuming the mass loss of ~ 3% for PBI (as shown by the pure PBI).

The effect of the acid doping on the film mechanical stability is investigated, and stress–strain plots at 35 and 100 °C are displayed in Fig. 2e and S1f, respectively. At both temperatures, the acid doping increases Young's modulus of the membranes because of the cross-linking (cf. Table S3). At 35 °C, the acid doping has a negligible effect on the yield strength except for PBI-PA$_{0.21}$, presumably because of the defects in PA$_{0.21}$. By contrast; at 100 °C, the acid doping decreases the yield strength, and increasing the temperature decreases Young's modulus and yield strain, reflecting that high temperature

weakens the H-bonds and partially breaks the cross-linking structure.[35, 36]

Fig. 2f shows that increasing the acid content increases the density (ρ_m), which can be described using an additive model:[25,29]

$$\frac{1}{\rho_m} = \frac{\omega_p}{\rho_p} + \frac{\omega_a}{\rho_a} = \frac{1}{\rho_p} + \left(\frac{1}{\rho_a} - \frac{1}{\rho_p}\right)\omega_a \qquad (2)$$

where ω_p and ω_a are the mass fraction of the PBI and acid in the complexes, respectively. ρ_p and ρ_a are the density of PBI and amorphous acid in the complex, respectively. The obtained ρ_a values (Table S1) are higher than the density of the pure crystalline acids measured by a pycnometer. For instance, TMA exhibits the ρ_a of 2.02 g/cm^3, much higher than its crystalline density (1.44 g/cm^3). The discrepancy can be ascribed to the tightened PBI structures and thus increased ρ_p with the increasing acid doping level. This phenomenon was also observed for PBI doped with other polyprotic acids.[24, 25] However, as the density of the amorphous acids is unknown, we do not have ways to obtain the actual values of ρ_p and ρ_a in these supramolecular assemblies.

Effect of the acid doping on H$_2$/CO$_2$ separation properties

Fig. 3a illustrates the effect of the PA doping level on pure-gas H$_2$/CO$_2$ separation properties at 35 °C. For each acid-doped samples, two or more films were tested to ensure the reproducibility of the data, and the difference is usually within 10% (cf. Table S4). Increasing the doping level decreases gas permeability and increases H$_2$/CO$_2$ selectivity, consistent with the decreased d-spacing and enhanced size-sieving ability. For instance, increasing the doping level from 0 to 0.49 increases H$_2$/CO$_2$ selectivity from 14 to 49. Similar trends are also observed for PBI-TMA and PBI-PMA (cf. Table S5).

Gas permeability (P_A) is a combination of solubility (S_A) and diffusivity (D_A), i.e., $P_A = D_A \times S_A$. Fig. 3b displays CO$_2$ sorption isotherms of the PBI-acid samples at 35 °C, which can be satisfactorily described using the dual-mode sorption model.[37] The values of the fitting parameters are recorded in Table S6. Fig. 3c demonstrates that increasing the PA doping level slightly decreases CO$_2$ solubility and dramatically decreases CO$_2$ diffusivity. For instance, as the PA doping level increases from 0 to 0.49, CO$_2$ solubility decreases from 2.4 to 1.8 cm^3(STP) cm^{-3} atm^{-1} by 25% while CO$_2$ diffusivity decreases from 5.1 × 10^{-10} to 3.7 × 10^{-11} cm^2 s^{-1} by more than one order of magnitude (cf. Table S7), demonstrating that the decreased permeability with the increasing acid doping level is primarily caused by the decreased diffusivity.[24, 25] Notably, the pure acid (such as TMA) has negligible CO$_2$ sorption due to their crystalline nature (cf. Table S7).
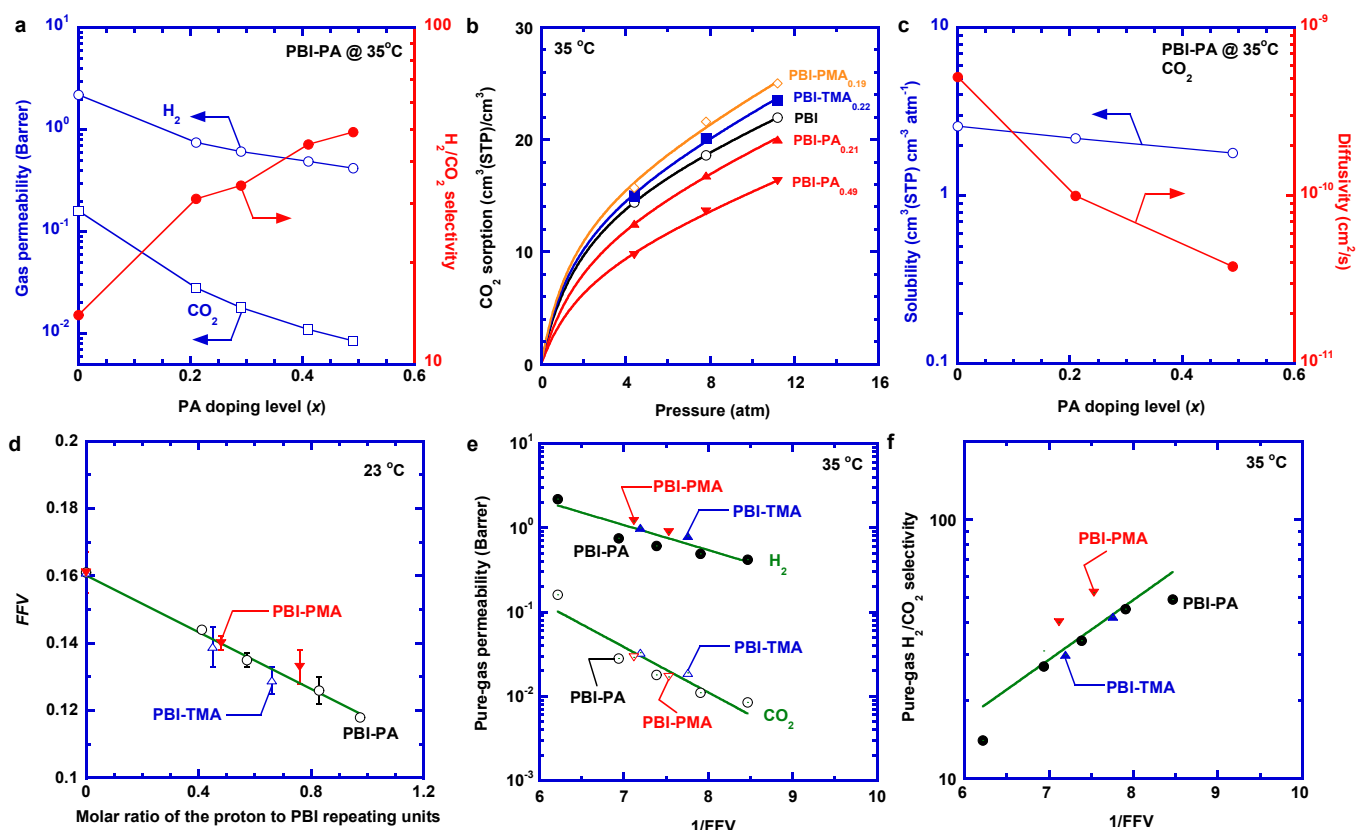
Fig. 3 Pure-gas transport properties of PBI-acid samples at 35 °C. Effect of the doping level on (a) H$_2$/CO$_2$ separation properties of PBI-PA, (b) CO$_2$ sorption isotherms, and (c) CO$_2$ solubility and diffusivity at ≈ 8 atm. Correlation of the *FFV* with (d) the molar ratio of the proton to PBI repeating units, (e) H$_2$ and CO$_2$ permeability, and (f) H$_2$/CO$_2$ selectivity. The lines in (e) and (f) are the best fits of the free volume model (cf. eq 4).

Gas diffusivity depends considerably on the amount of free volume in the polymers, which is characterized by fractional free volume (*FFV*) defined by the following equation:

$$FFV = \frac{V - V_0}{V} = \frac{V - 1.3V_w}{V} \qquad (3)$$

where *V* and V_w are the specific volume and van der Waals volume, respectively. V_w is estimated by the group contribution method. Increasing the acid doping level decreases the *FFV* (cf. Table S2) due to the cross-linking of the polymer chains by these polyprotic acids. At the same doping level, PBI-PMA and PBI-TMA exhibit similar *FFV* values, which are much lower than those for PBI-PA (cf. Fig. S3a). Fig. 3d illustrates that the *FFV* decreases linearly with the increasing proton content in the PBI-acid (defined as the molar ratio of the proton and PBI repeating units). A similar correlation can also be observed for PBI doped with other polyprotic acids (Fig. S3b),[24, 25] suggesting the dominant impact of the cross-linking. The decreased free volume with the addition of small acid molecules can also be partially ascribed to the antiplasticization effect, where the small molecules fill up the Langmuir sites and microvoids.[38] However, both mechanisms can not be decoupled. Nevertheless, it does not affect the data analysis and interpretation, as shown below.

Because the acid doping exerts much more significant impact on gas diffusivity than solubility, the free volume model can be expressed by eq 3:[39]

$$P_A = A_p \exp\left(-\frac{B_p}{FFV} \right) \qquad (4)$$

where A_P and B_P are constants. Fig. 3e displays that both H_2 and CO_2 permeability of PBI-PA, PBI-TMA, and PBI-PMA are well correlated with the *FFV* using the B_P value of 0.68 for H_2 and 1.2 for CO_2, consistent with their molecular size. H_2/CO_2 selectivity can also be satisfactorily described by the free volume model (cf. Fig. 3f), though PBI-PMA appears to show higher selectivity than expected based on the model.

Effect of temperature on H_2/CO_2 separation properties

Fig. 4a and S6a present the effect of the temperature on the H_2 and CO_2 permeability in PBI-PA samples, respectively. Increasing the temperature increases gas permeability, which can be described using the Arrhenius equation:
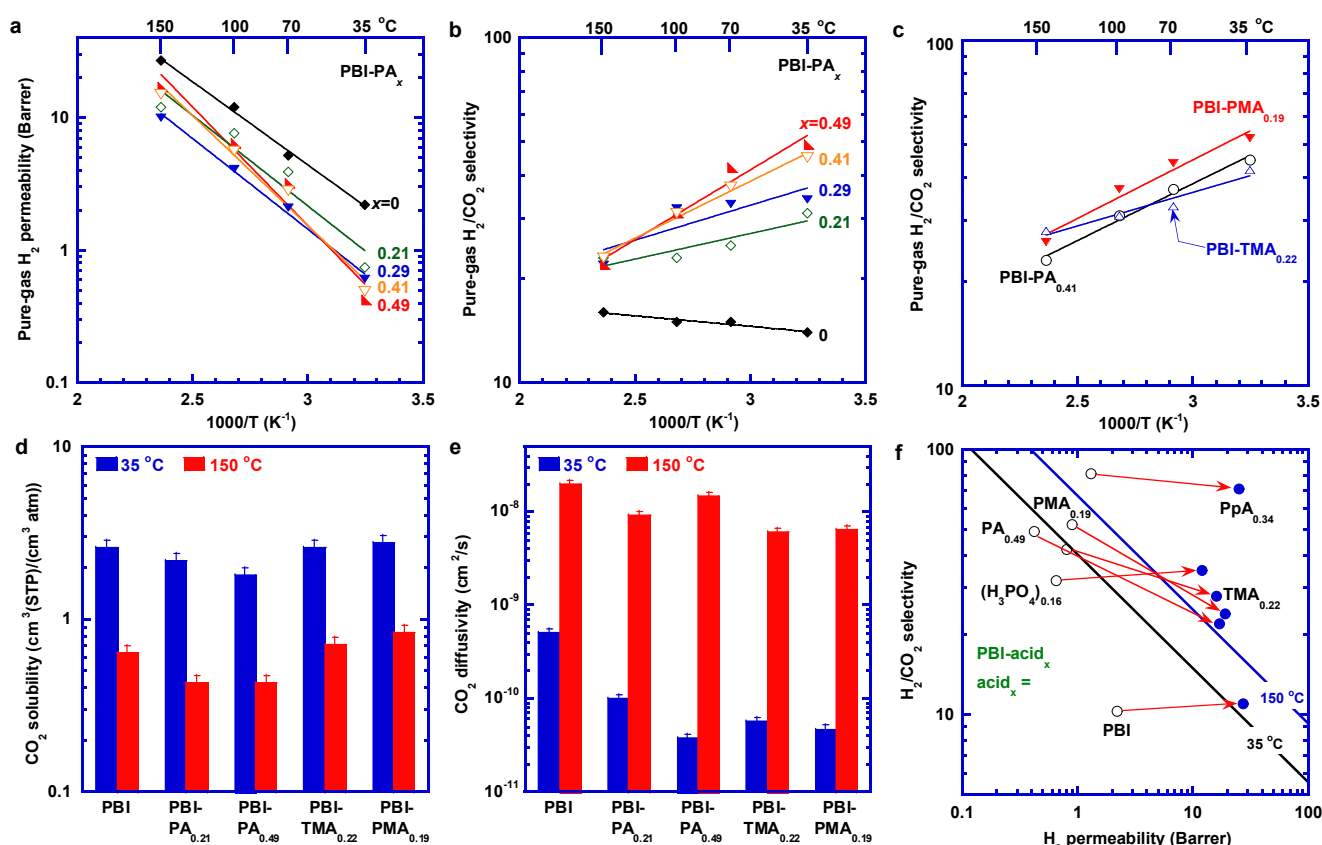
Fig. 4 Effect of the temperature on (a) pure-gas H_2 and CO_2 permeability and (b) H_2/CO_2 selectivity of PBI-PA. (c) Comparison of the H_2/CO_2 selectivity among PBI-PA$_{0.42}$, PBI-TMA$_{0.22}$, and PBI-PMA$_{0.19}$ with similar ratios of proton to PBI repeating units (0.66 – 0.84). The lines are the best fits of the Arrhenius Equation (eq 5). Effect of the acid doping on (d) CO_2 solubility and (e) CO_2 diffusivity at ≈ 8 atm and 35 and 150 °C. (f) Comparison of the effect of temperature on pure-gas H_2/CO_2 separation properties of the PBI doped by various acids such as PA, TMA, PMA, H_3PO_4, and PPA in Robeson's 2008 upper bound plot.

$$P_A = P_{A,0} \exp\left(\frac{-E_{P,A}}{RT}\right) \qquad (5)$$

where $P_{A,0}$ is a pre-exponential factor (Barrer), R is the gas constant, and $E_{P,A}$ is the activation energy for gas permeation (kJ/mol). The values of the $P_{A,0}$ and $E_{P,A}$ are listed in Table S8. For PBI-PA, $E_{P,A}$ value increases with the increasing doping level as a result of the decreased free volume. For example, $E_{P,A}$ for H_2 increases from 24 kJ/mol for PBI to 34 kJ/mol for PBI-$PA_{0.49}$. Likewise, $E_{P,A}$ of CO_2 increases from 23 kJ/mol for PBI to 42 kJ/mol for PBI-$PA_{0.49}$. The PBI-acid exhibits lower $E_{P,A}$ values for H_2 than CO_2, and the difference increases with the increasing doping level because of the enhanced size-sieving ability, which decreases the permeability of the larger molecule (i.e., CO_2) more than the smaller H_2 molecule. PBI-$PMA_{0.19}$ displays higher $E_{P,A}$ values for both H_2 and CO_2 than PBI-$PA_{0.21}$ and PBI-$TMA_{0.22}$, probably because of the higher proton content in PBI-$PMA_{0.19}$ (with the molar ratio of proton to PBI repeating units of 0.78).

Table S5 shows that increasing the TMA doping level decreases gas permeability and increases H_2/CO_2 selectivity at 150 °C, and increasing the PMA doping level from 0.12 to 0.19 has essentially no impact on the H_2/CO_2 separation properties at 150 °C. By contrast, Fig. S4a shows that the gas permeability of PBI-PA at 150 °C decreases with increasing the acid doping level before increasing because of the interplay between the cross-linking and plasticization caused by the acids. At the low loadings, the cross-linking dominates, and thus, gas permeability decreases. On the other hand, at the doping levels above 0.29, the high temperature leads to a high concentration of free acids,[25] plasticizing the PBI and thus increasing gas permeability.

Fig. 4b presents the effect of temperature on H_2/CO_2 selectivity. PBI displays H_2/CO_2 selectivity independent of the temperature. By contrast, the aromatic carboxylic acid-doped PBI show H_2/CO_2 selectivity decreasing with increasing temperature. For instance, as the temperature increases from 35 to 150 °C, H_2/CO_2 selectivity decreases from 50 to 22 for PBI-$PA_{0.49}$ and from 52 to 26 for PBI-$PMA_{0.19}$. This may be caused by the weakened cross-linking between the carboxylic acid and imidazole rings at higher temperatures, decreasing the size-sieving ability.

Fig. 4c compares the H_2/CO_2 selectivity among three samples with a similar molar ratio of proton to PBI repeating units (PBI-$PA_{0.422}$, PBI-$TMA_{0.22}$, and PBI-$PMA_{0.19}$) at temperatures from 35 to 150 °C. PBI-$TMA_{0.22}$ exhibits the lowest selectivity at 35 °C due to the lowest molar ratio but the highest selectivity at 150 °C, presumably because of its most symmetric planar positions of protons, leading to the most compact structure. This result is also consistent with the best thermal stability of TMA among the three acids (Figure S1c).

Fig. 4d shows that increasing temperature decreases CO_2 solubility. Interestingly, at 35 °C, increasing the PA doing level appears to decrease CO_2 solubility, while doping with TMA and PMA has minimal impact on CO_2 solubility. Fig. 4e displays that increasing the acid doping level decreases CO_2 diffusivity due to the decreased free volume for PBI-$PA_{0.21}$, PBI-$TMA_{0.22}$, and PBI-$PMA_{0.19}$ at 35 and 150 °C. The acid doping exhibits less influence on the CO_2 diffusivity at 150 °C than 35 °C, confirming the weakened cross-linking at higher temperatures. For example, doping the PBI with TMA at x = 0.22 decreases CO_2 diffusivity by ~90% from 5.1×10^{-10} to 5.6×10^{-11} cm^2/s at 35 °C and only by 70% from 2.0×10^{-8} to 6.0×10^{-9} cm^2/s at 150 °C

(cf. Table S7). The difference further validates the weakened interactions and increased content of free acid molecules and thus plasticization at higher temperatures.[24]

Fig. 4f compares pure-gas H_2/CO_2 separation properties of typical acid-doped PBI films with the upper bounds at 35 and 150 °C, including PBI-$PA_{0.49}$, PBI-$TMA_{0.22}$, and PBI-$PMA_{0.19}$. At 35 °C, PBI-$PMA_{0.19}$ shows the best H_2/CO_2 separation performance above the upper bound, followed by PBI-$TMA_{0.22}$ and then PBI-$PMA_{0.19}$, suggesting that higher proton contents in PBI improve H_2/CO_2 separation performance. This can also be concluded from the comparison between PBI-$(H_3PO_4)_{0.16}$ and PBI-$PpA_{0.34}$. On the other hand, in contrast to the aromatic acid-doped PBI films, PBI, PBI-$(H_3PO_4)_{0.16}$, and PBI-$PpA_{0.34}$ display H_2/CO_2 selectivity independent of temperature.[5, 24] Noticeably, the H-bond energy for $[N\cdots H\cdots N]^+$ in PBI and P-OH$\cdots$O=P in PBI-H_3PO_4 is 63-167 kJ/mol, much stronger than N-H$\cdots$O=C (17-63 kJ/mol) and C-H$\cdots$O (<17 kJ/mol).[40] The effect of temperature on this H-bond energy can be studied to elucidate its impact on the H_2/CO_2 separation properties. However, it is beyond the scope of this study.

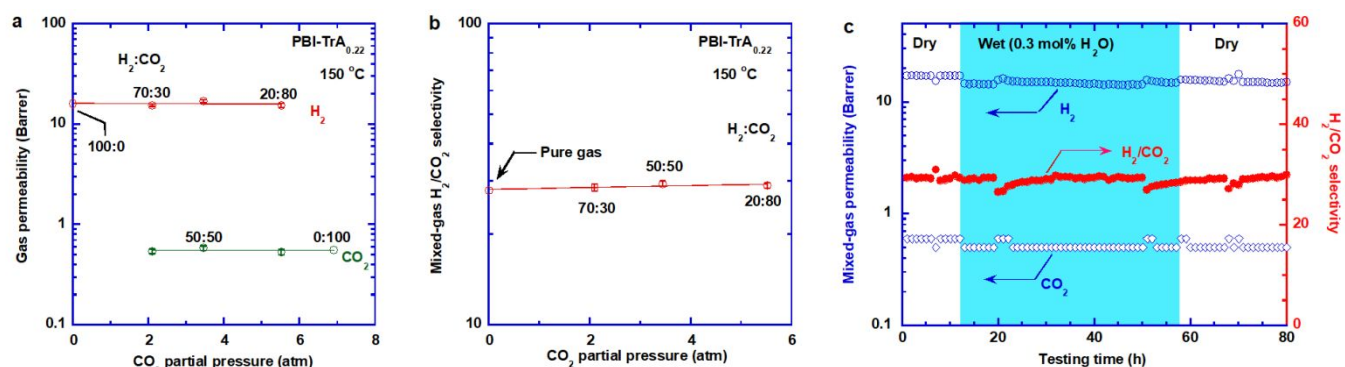### Superior H_2/CO_2 separation properties

PBI-$TMA_{0.22}$ with the best combined H_2 permeability and H_2/CO_2 selectivity at 150 °C was evaluated using three gas mixtures of H_2:CO_2 with molar ratios of 70:30, 50:50, and 20:80 at 150 °C and ≈ 7 atm. Fig. 5a shows that mixed-gas permeability is similar to the pure-gas permeability and independent of the feed CO_2 partial pressure. CO_2 plasticization is minimal due to the low CO_2 sorption at high temperatures. As such, mixed-gas H_2/CO_2 selectivity is almost the same as pure-gas selectivity and independent of the CO_2 partial pressure (Fig. 5b).

PBI-$TMA_{0.22}$ was also challenged with a mixture containing H_2:CO_2 of 50:50 at 150 °C and ≈ 7 atm for a longer-term test. The film demonstrates robust H_2/CO_2 separation properties at the first 12 h with H_2 permeability of 17 Barrer and H_2/CO_2 selectivity of 29 (Fig. 5c). When the 0.3 mol% water vapor is introduced to the feed, the gas permeability slightly decreases, but H_2/CO_2 selectivity remains almost the same. When the feed gas is switched back to the dry gas mixture, the gas permeability recovers to its original values. Nevertheless, for this material to be further considered for practical applications, the effects of higher water vapor partial pressure and higher temperatures on the long-term H_2/CO_2 separation performance need to be assessed.

Fig. 6 compares the H_2/CO_2 separation performance of the three aromatic acid-doped PBI films with leading cross-linked polymers for H_2/CO_2 separation.[12-14, 20, 25, 41-44] Cross-linked polymers via interfacial polymerization (IP) show excellent H_2/CO_2 separation performance due to the high cross-linking degrees.[42-44] Compared to other cross-linked PBIs, PBI-$TMA_{0.22}$ and PBI-$PMA_{0.19}$ display one of the best combinations of H_2 permeability and H_2/CO_2 selectivity.

Conclusion

We systematically investigated three series of supramolecular assemblies based on PBI and three aromatic polycarboxylic acids (PA, TMA, and PMA) for their structures and H_2/CO_2 separation performance. These acids have similar structures but different amounts of the -COOH groups, and thus, the resulting assemblies are ideal models to interpret the effect of the dynamic non-covalent

Fig. 5 Superior H_2/CO_2 separation performance of PBI-TMA$_{0.22}$. Effect of the feed CO_2 partial pressure on (a) mixed-gas H_2 and CO_2 permeability and (b) mixed-gas H_2/CO_2 selectivity at ≈ 7 atm and 150 °C. (c) Long-term stability in dry–wet–dry conditions with H_2:CO_2 of 50:50 at ≈ 7 atm and 150 °C for 80 h.
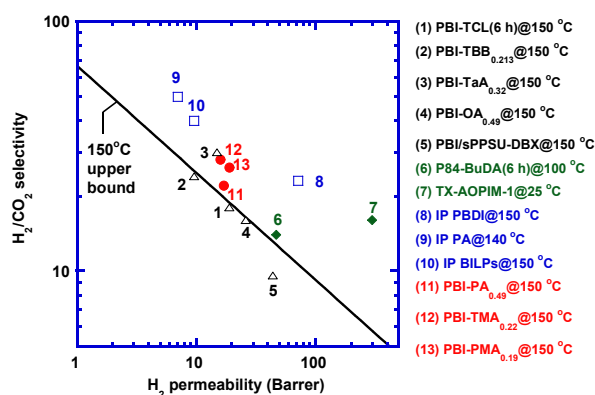
Fig. 6 Comparison between the PBI-based supramolecular assemblies in this study and other leading polymeric membrane materials: PBI-TCL (6 h),[13] PBI-TBB$_{0.213}$,[12] PBI-TaA$_{032}$,[25] PBI-OA$_{0.49}$,[25] PBI/sPPSU-DBX,[41] P84-BuDA (6 h),[14] TX-AOPIM-1,[20] IP PBDI,[42] IP PA,[43] and IP BILPs.[44]

bonds on the gas separation properties. The acids complex with PBI through the H-bonds and proton transfer, as evidenced by the transformation of the acids from the crystalline state in the pure form to the amorphous state in the assemblies, FTIR spectra, and thermomechanical properties. The acid doping increases density and decreases the *FFV* and thus gas diffusivity and permeability, resulting in increased H_2/CO_2 selectivity. The decreased *FFV* and permeability can be correlated with the molar ratio of the protons and PBI repeating units in the assemblies. Increasing the temperature decreases H_2/CO_2 selectivity for the PBI doped with carboxylic acids because of the weakened interactions at high temperatures and thus more open structures. This behavior is different from PBI and PBI doped with H_3PO_4 and PpA. Among the PBI-PA, PBI-TMA, and PBI-PMA samples, PBI-TMA$_{0.22}$ shows the best pure-gas H_2/CO_2 separation performance and was further tested with gas mixtures at various feed compositions and pressures and even in the presence of water vapor. This example supramolecular assembly demonstrates robust H_2/CO_2 separation performance above Robeson's upper bound. This work may stimulate the interest in tailoring non-covalent

bonds to achieve robust gas separation performance with superior mechanical properties.

Author contributions:

Conceptualization: L.H., H.L.
Methodology: L.H., V.B., S.F., W.G., S.P., D.Y.
Investigation: L.H., H.L.
Visualization: L.H., H.L.
Supervision: H.L.
Writing—original draft: L.H.
Writing—review & editing: L.H., V.B., S.F., W.G., S.P., Y.D., H.L.

Conflicts of interest

There are no conflicts to declare.

Acknowledgements

References

1.	Y. Han and W. S. Ho, *J. Membr. Sci.*, 2021, **628**, 119244.
2.	L. Hu, S. Pal, H. Nguyen, V. Bui and H. Lin, *J. Polym. Sci.*, 2020, **58**, 2467-2481.
3.	H. Park, J. Kamcev, L. M. Robeson, M. Elimelech and B. D. Freeman, *Science*, 2017, **356**, eaab0530.
4.	H. Lin, *Curr. Opin. Chem. Eng.*, 2014, **4**, 54-61.
5.	L. Hu, V. T. Bui, A. Krishnamurthy, S. Fan, W. Guo, S. Pal, X. Chen, G. Zhang, Y. Ding, R. P. Singh, M. Lupion and H. Lin, *Sci. Adv.*, 2022, **8**, abl8160.
6.	L. Zhu, L. Huang, S. R. Venna, A. Blevins, Y. Ding, D. Hopkinson, M. T. Swihart and H. Lin, *ACS Nano*, 2021, **15**, 12119-12128.
7.	L. F. Villalobos, M. T. Vahdat, M. Dakhchoune, Z. Nadizadeh, M. Mensi, E. Oveisi, D. Campi, N. Marzari and K. V. Agrawal, *Sci. Adv.*, 2020, **6**, eaay9851.
8.	L. Zhu, D. Yin, Y. Qin, S. Konda, S. Zhang, A. Zhu, S. Liu, T. Xu, M. T. Swihart and H. Lin, *Adv. Funct. Mater.*, 2019, **29**,

9. K. A. Stevens, J. D. Moon, H. Borjigin, R. Liu, R. M. Joseph, J. S. Riffle and B. D. Freeman, *J. Membr. Sci.*, 2020, **593**, 117427.
10. X. Li, R. P. Singh, K. W. Dudeck, K. A. Berchtold and B. C. Benicewicz, *J. Membr. Sci.*, 2014, **461**, 59-68.
11. L. Zhu, M. Omid and H. Lin, in *Membranes for Gas Separations*, ed. M. A. Carreon, World Scientific, 2017, vol. 1, pp. 243-270.
12. A. Naderi, A. A. Tashvigh and T. S. Chung, *J. Membr. Sci.*, 2019, **572**, 343-349.
13. L. Zhu, M. Swihart and H. Lin, *J. Mater. Chem. A*, 2017, **5**, 19914-19923.
14. M. Omidvar, C. M. Stafford and H. Lin, *J. Membr. Sci.*, 2019, **575**, 118-125.
15. S. Japip, K. S. Liao and T. S. Chung, *Adv. Mater.*, 2017, **29**, 1603833.
16. H. Wang, D. R. Paul and T. Chung, *J. Membr. Sci.*, 2013, **430**, 223-233.
17. B. Low, Y. Xiao, T. Chung and Y. Liu, *Macromolecules*, 2008, **41**, 1297-1309.
18. L. Shao, T. Chung, S. Goh and K. Pramoda, *J. Membr. Sci.*, 2005, **256**, 46-56.
19. F. Li, Y. Xiao, Y. K. Ong and T. S. Chung, *Adv. Energy Mater.*, 2012, **2**, 1456-1466.
20. M. Huang, K. Lu, Z. Wang, X. Bi, Y. Zhang and J. Jin, *ACS Sustain. Chem. Eng.*, 2021, **9**, 9426-9435.
21. P. Song and H. Wang, *Adv. Mater.*, 2020, **32**, 1901244.
22. C. Ma and J. J. Urban, *Adv. Funct. Mater.*, 2019, **29**, 1903243.
23. W. Han, M. Yin, W. Zhang, Z. Liu, N. Wang, K. Yong and Q. An, *Adv. Sci.*, 2021, **8**, 2102594.
24. L. Zhu, M. Swihart and H. Lin, *Energy Environ. Sci.*, 2018, **11**, 94-100.
25. L. Hu, V. T. Bui, L. Huang, R. P. Singh and H. Lin, *ACS Appl. Mater. Interfaces*, 2021, **13**, 12521-12530.
26. S. Zieba, A. Dubis, P. Lawniczak, A. Gzella, K. Pogorzelec-Glaser and A. Lapinski, *Electrochim. Acta*, 2019, **306**, 575-589.
27. X. Chen, S. Jin, H. Zhang, X. Xiao, B. Liu and D. Wang, *J. Mol. Struct.*, 2017, **1144**, 514-528.
28. D. R. Trivedi, A. Ballabh and P. Dastidar, *CrystEngComm*, 2003, **5**, 358-367.
29. L. Hu, J. Liu, L. Zhu, X. Hou, L. Huang, H. Lin and J. Cheng, *Sep. Purif. Technol.*, 2018, **205**, 58-65.
30. V. Chithambaram, S. J. Das, S. Krishnan, M. B. Ahamed and R. A. Nambi, *Eur. Phys. J. Appl. Phys.*, 2013, **64**, 20201.
31. S. Han, J. Lee, K. Lee, H. Park and Y. Lee, *J. Membr. Sci.*, 2010, **357**, 143-151.
32. T. Yang, Y. Xiao and T. S. Chung, *Energy Environ. Sci*, 2011, **4**, 4171-4180.
33. R. M. Joseph, M. M. Merrick, R. Liu, A. C. Fraser, J. D. Moon, S. R. Choudhury, J. Lesko, B. D. Freeman and J. S. Riffle, *J. Membr. Sci.*, 2018, **564**, 587-597.
34. N. P. Panapitiya, S. N. Wijenayake, D. D. Nguyen, Y. Huang, I. H. Musselman, K. J. Balkus and J. P. Ferraris, *ACS Appl. Mater. Interfaces*, 2015, **7**, 18618-18627.
35. E. Mahdi and J.-C. Tan, *J. Membr. Sci.*, 2016, **498**, 276-290.
36. Z. P. Smith, J. E. Bachman, T. Li, B. Gludovatz, V. A. Kusuma, T. Xu, D. P. Hopkinson, R. O. Ritchie and J. R. Long, *Chem. Mater.*, 2018, **30**, 1484-1495.
37. Z. P. Smith, R. R. Tiwari, T. M. Murphy, D. F. Sanders, K. L. Gleason, D. R. Paul and B. D. Freeman, *Polymer*, 2013, **54**, 3026-3037.
38. Y. Maeda and D. R. Paul, *J. Polym. Sci. B: Polym. Phys.*, 1987, **25**, 1005-1016.
39. J. Park and D. R. Paul, *J. Membr. Sci.*, 1997, **125**, 23-39.
40. G. R. Desiraju and T. Steiner, *The Weak Hydrogen Bond in Structural Chemistry and Biology*, Oxford University Press, Oxford, 2001.
41. A. Naderi, A. A. Tashvigh, T. S. Chung, M. Weber and C. Maletzko, *J. Membr. Sci.*, 2018, **563**, 726-733.
42. M. Shan, X. Liu, X. Wang, Z. Liu, H. Iziyi, S. Ganapathy, J. Gascon and F. Kapteijn, *J. Mater. Chem. A*, 2019, **7**, 8929-8937.
43. Z. Ali, F. Pacheco, E. Litwiller, Y. Wang, Y. Han and I. Pinnau, *J. Mater. Chem. A*, 2018, **6**, 30-35.
44. M. Shan, X. Liu, X. Wang, I. Yarulina, B. Seoane, F. Kapteijn and J. Gascon, *Sci. Adv.*, 2018, **4**, eaau1698.